Radiomics-based comparison of MRI and CT for differentiating pleomorphic adenomas and Warthin tumors of the parotid gland: a retrospective study

Yuebo Liu, MD,[a] Jiabao Zheng, MD,[b] Xiaoping Lu, MD,[c] Yao Wang, MD,[d] Fantai Meng, PhD,[e] Jizhi Zhao, MD,[a] Chunlan Guo, MD,[a] Lijiang Yu, MD,[a] Zhihui Zhu, MD,[a] and Tao Zhang, MD[a]

Objective. The objective of this study was to compare the diagnostic performance of magnetic resonance imaging (MRI) and computed tomography (CT) in differentiating pleomorphic adenomas from Warthin tumors using radiomics.

Study Design. We retrospectively reviewed 626 patients who underwent preoperative MRI or CT for parotid tumor diagnosis. Patient groups were balanced by propensity score matching (PSM) and 123 radiomic features were extracted from tumor images. Radiomic signatures (rad-scores) were generated using a least absolute shrinkage and selection operator logistic regression model. The Canny edge detector was used to define tumor borders (border index). The diagnostic performance of rad-score and border index before and after PSM was evaluated with area under the receiver operating characteristic curve analysis.

Results. For differentiation of pleomorphic adenomas and Warthin tumors, rad-score and border index areas under the curve for MRI after PSM were 0.911 (95% confidence interval [CI], 0.871-0.951) and 0.716 (95% CI, 0.646-0.787), respectively; those for CT were 0.876 (95% CI, 0.829-0.923) and 0.608 (95% CI, 0.527-0.690), respectively. Tumor border index on MRI, but not CT, had superior diagnostic performance ($P < .05$); MRI- and CT-based rad-scores showed similar performance ($P > .05$).

Conclusions. MRI is superior to CT for tumor margin examination; however, the radiomics features of both modalities showed no difference. (Oral Surg Oral Med Oral Pathol Oral Radiol 2021;131:591−599)

Salivary gland tumors usually present as painless enlarged masses, the majority of which occur in the parotid glands, and 80% of these tumors are benign. Pleomorphic adenomas (PAs) and Warthin tumors (WTs) are the most common benign tumors of the parotid gland, whereas other tumors are relatively rare.[1] PAs are characterized by the neoplastic proliferation of parenchymatous glandular cells along with myoepithelial components. WTs are histopathologically composed of a benign cyst containing abundant lymphocytes and lymph node−like stroma.[2] Both PAs and WTs exhibit similar clinical characteristics, making it difficult to distinguish them. A differential diagnosis of both parotid tumors is important because it affects treatment planning and disease prognosis.[3] For instance, PAs can grow larger or become malignant (nearly 25% exhibit transformation into carcinoma ex pleomorphic adenoma) if excision is delayed and can recur after surgery;[4-6] thus, partial superficial parotidectomy is recommended for patients with PAs.[7,8] In contrast, malignant transformation of WTs is a rare event that occurs in fewer than 1% of cases, and extracapsular dissection is used for patients with WTs.[9] Preoperative differentiation of PAs and WTs would be of great importance when considering an optimal individualized operative program and would provide helpful information for preoperative patient counseling.

A multitude of diagnostic tests, typically magnetic resonance imaging (MRI) and computed tomography (CT), are available to aid in the diagnosis of parotid tumors. MRI provides excellent resolution of the soft tissues, with additional information on the organization, density, microstructure, and microcirculation of the tissue,[10,11] and CT specifically defines the anatomic localization and extent of the parotid mass.[12] Several imaging features, such as uniformity of internal signals inside the tumor and definition of the borders, are reported to be helpful in differentiating PAs and WTs.[2,13,14] However, the conclusions are still subjective and mainly depend on the physician's experience.[15]

Statement of Clinical Relevance

In radiomics evaluation, magnetic resonance imaging was more informative than computed tomography with respect to tumor margin appearance for diagnosing pleomorphic adenomas and Warthin tumors, which could provide reference for doctors to choose proper preoperative imaging examination methods in clinical practice.

[a]Department of Stomatology, Peking Union Medical College Hospital, Peking Union Medical College, Chinese Academy of Medical Sciences, Beijing, China.
[b]Department of Implant Dentistry, Beijing Stomatological Hospital, Capital Medical University, Beijing, China.
[c]Department of Radiology, Peking Union Medical College Hospital, Peking Union Medical College, Chinese Academy of Medical Sciences.
[d]Department of Stomatology, Beijing Fangshan District Liangxiang Hospital, Beijing, China.
[e]Ocean and Civil Engineering, School of Naval Architecture, Shanghai Jiao Tong University, Shanghai, China.
Received for publication Sep 9, 2020; returned for revision Dec 16, 2020; accepted for publication Jan 9, 2021.

2212-4403/$-see front matter
https://doi.org/10.1016/j.oooo.2021.01.014

Radiomics is a field of medical imaging that involves the detection and quantification of mathematical patterns in digital images by using computer-assisted techniques. Parameters derived from radiomic analysis are able to reflect the gray-level distribution of pixels.[16] First-order statistical outputs describe the distribution of pixel values (gray-level histograms). Second-order statistical outputs describe relations between pixels or voxels (e.g., co-occurrence matrix and run-length matrix). Image filtering and wavelet transformations also generate additional features.[17] The parameters above can provide a theoretical basis for identifying tiny differences in tumors on images. Currently, with the development of artificial intelligence and algorithms, more attention is being paid to improving preoperative diagnostic accuracy for parotid tumors with a computer-assisted quantitative image evaluation.[18-21]

However, there is a paucity of literature on quantitative comparisons of preoperative MRI and CT to diagnose parotid tumors, especially from the perspective of radiomics.[22,23] Thus, there is no consensus on the most informative imaging technique for presurgical diagnosis of parotid tumors.

In this retrospective study, we aimed to compare the diagnostic performance of MRI and CT to preoperatively examine parotid tumors. Propensity score matching (PSM) was used to balance patient groups when adjusting for possible confounding factors. We primarily considered 2 aspects when evaluating the preoperative images: the internal architecture of the lesion, which was based on the extraction of a large number of quantitative features from the MRI and CT images, and the appearance of the tumor margin, which refers to the ability of the imaging modality to differentiate the actual border or margin of the parotid mass from the surrounding normal tissue. In this study, we used Canny edge detection to quantify the description of the tumor margin appearance,[24] with the aim of achieving more objective results.

The objective of this study was to compare the measures of internal architecture derived from radiomics and tumor borders derived from Canny edge detection in distinguishing PA and WT on MR and CT images. The null hypothesis stated that neither parameter would be significantly different between PA and WT.

MATERIALS AND METHODS

Patients

This retrospective study was approved by the institutional review board of our hospital (Peking Union Medical College Hospital) and followed the principles of the Declaration of Helsinki. Data for 659 patients who underwent MRI or CT for presurgical evaluation of parotid tumors from January 2013 to January 2020 were collected and reviewed. Only patients who underwent surgery and were diagnosed with PA or WT based on histopathological examination of surgical resection specimens were included. The exclusion criteria were as follows: (1) lack of MRI or CT images or clinical data (n = 22); (2) maximum lesion diameter less than 5 mm (n = 3); and (3) presence of severe motion artifacts or obvious noise in the MRI or CT images (n = 8). Finally, 626 patients were included in the study. Presurgical clinical characteristics collected from the hospital information system included age, sex, disease duration, lesion size, symptom (with/without pain), smoking history, systemic disease, tumor hardness, tumor mobility, and tumor location.

MRI and CT Protocols

MRI examinations were performed on a 3 T scanner (MAGNETOM Skyra, Siemens Healthineers, Erlangen, Germany) with a 20-channel head/neck coil. The standard protocol for MRI of parotid lesions included the following: (1) axial T1-TSE (turbo spin echo) sequence, repetition time (TR)/echo time (TE) = 600/8.7 ms, and matrix = 269 × 384; and (2) axial T2-TSE sequence, TR/TE = 5000/95 ms, and matrix = 314 × 448. All images were acquired with a slice thickness of 4 mm, a slice number of 20, and a field of view of 220 × 220 mm.

CT scans were performed using a 64-slice CT scanner (Discovery CT750 HD, GE Medical Systems, Waukesha, WI, USA) with the following parameters: 120 kV; smart mA (50-600 mA); slice thickness and interval for axial images 3.750 mm/3.750 mm. The scanning area ranged from 1 cm below the aortic arch to the top of the head. For contrast-enhanced CT scanning, the patients were administered a total of 60 to 100 mL (1.25 mL per kg of weight) of nonionic iodinated contrast material (320 mg/mL; Iopamidol, JiangSu HengRui Pharmaceutical, Jiangsu, China). The contrast medium was injected at a rate of 2.0 to 2.5 mL/s using a power injector. Contrast-enhanced CT images were acquired 40 s after the contrast material was injected.

PSM

A detailed assessment of each individual was performed and the propensity score was calculated via a multiple-factor logistic regression model. A caliper of 0.2 standard deviations of the logit of the propensity score was applied. We used simple 1:1 matching based on the nearest-neighbor matching principle and the "nonreplacement principle," which prohibits items from being selected multiple times. The standardized mean differences (SMDs) were then calculated. Clinical factors were considered comparable when the SMD was below 0.10. In total, 4 patient cohorts were obtained: group A, MRI before PSM; group B, CT before PSM; group C, MRI after PSM; and group D, CT after PSM.

Canny Edge Detection

Canny edge detection was performed as follows: (1) images were smoothed to eliminate noise, (2) regions with high spatial derivatives were highlighted, (3) pixels that were not at the maximum in the highlighted regions were suppressed, and (4) the gradient array was further reduced by hysteresis.[25] Hysteresis was used to track the remaining nonsuppressed pixels. Two thresholds were used: If the magnitude was below the lower threshold (Th1), edge detection was set to 0 (defined as a non-edge); conversely, if the magnitude was above the higher threshold (Th2), it was set as an edge. If the magnitude ranged between the 2 thresholds, it was set to 0 unless there was a path from the pixel to another with a gradient above Th2. The parameters for detecting the whole tumor border (B_1) were 40/100 (Th1/Th2), and the parameters for detecting a well-defined border (B_2) were 60/120 (Th1/Th2). The tumor border (border index) was quantitatively defined as the length of B_2 divided by B_1.

Radiomic Feature Extraction/Selection and Radiomics Signature Building

Texture analysis was performed using MaZda statistical texture analysis software (version 4.6, Technical University of Lodz, Institute of Electronics). The largest slice of the lesion was selected for image analysis. The Canny edge detection algorithm was used to segment the radiologic images of the parotid lesions, as aforementioned. After segmentation, 30 texture features were extracted: (1) 5 histogram features, (2) 11 gray-level co-occurrence matrix features, (3) 5 gray-level run-length features, (4) 5 gray-level gradient matrix features, and (5) 4 wavelet transform features. A more detailed description of their computation has been reported previously.[26] To diminish the influence of contrast and brightness variations, image gray-level intensity was normalized in the range of $\mu - 3\,\delta$, $\mu + 3\,\delta$ (μ, mean gray-level value; δ, standard deviation of the mean). There was a risk of overfitting due to the complexity of the radiomic features. A least absolute shrinkage and selection operator (LASSO) logistic regression model was used to identify the most valuable predictive features and build a radiomic signature. We used 10-fold cross-validation in the LASSO model for the selection of the conditioning parameters (λ). A radiomic score (rad-score) was computed for each patient using a linear combination of selected features weighted by their respective coefficients.[27]

Statistical Analysis

All statistical analyses were conducted using R software (version 3.6.3; R Foundation, Vienna, Austria). Canny edge detection was performed using MATLAB R2018 b (MathWorks, Natick, MA, USA). The lengths of B_1 and B_2 were calculated using Image-Pro Plus 6.0 (Media Cybernetics, Rockville, MD, USA). Receiver operating characteristic (ROC) curves and areas under the ROC curves (AUCs) were analyzed to assess the diagnostic performance of the rad-score and border index. The AUC cutoff values were established by calculating the maximal Youden index (sensitivity + specificity − 1). A paired DeLong test was performed to compare the diagnostic performance of MRI and CT after PSM. All reported statistical significance levels were 2-sided, and significance was set at $P < .05$.

RESULTS

Of the 626 patients who underwent surgical resection of their tumors with a confirmed histopathological diagnosis of PA or WT, 334 (53.4%) underwent MRI as the preoperative imaging examination for detecting parotid tumors and therefore comprised group A. Of these 334 patients, 236 were diagnosed with PA and 98 with WT. The remaining 292 patients (46.6%) underwent CT imaging preoperatively and comprised group B. Of these 292 patients, 168 were diagnosed with PA and 124 with WT. After PSM, 117 patients with PA and 80 patients with WT were included in both group C and group D, for a total of 197 patients in each of these groups.

The baseline characteristics of the patients with PA and WT are listed in Supplementary Tables S1 and S2 (available at [URL/link]), respectively. Before PSM, group A (MRI) and group B (CT) in the PA cohort differed by more than 0.1 SMD in tumor hardness, tumor mobility, age, systemic disease, lesion size, and disease duration, in descending order of SMD. Similarly, the groups in the WT cohort differed by more than 0.1 SMD in tumor mobility, tumor hardness, disease duration, lesion size, and age, also in descending order of SMD. After PSM, the patients in group C (MRI) and group D (CT) were similar regarding all of the 10 baseline covariates (Supplementary Tables S1 and S2). PSM reduced the SMDs for all observed covariates to below 10% of their absolute values, having demonstrated substantial improvement in the covariate balance between patients who underwent MRI and those who underwent CT (Figure 1).

We selected λ values of 0.040, 0.053, 0.059, and 0.129 in the LASSO model using a 10-fold cross-validation approach to identify the optimal subsets of radiomic features. At these values, the 123 extracted radiomic features were reduced in groups A and C (the MRI groups) to 9 and 11 potential predictors, respectively, with nonzero coefficients. The number of features remaining in groups B and D (the CT groups) was 2 and 3, respectively (Figure 2).

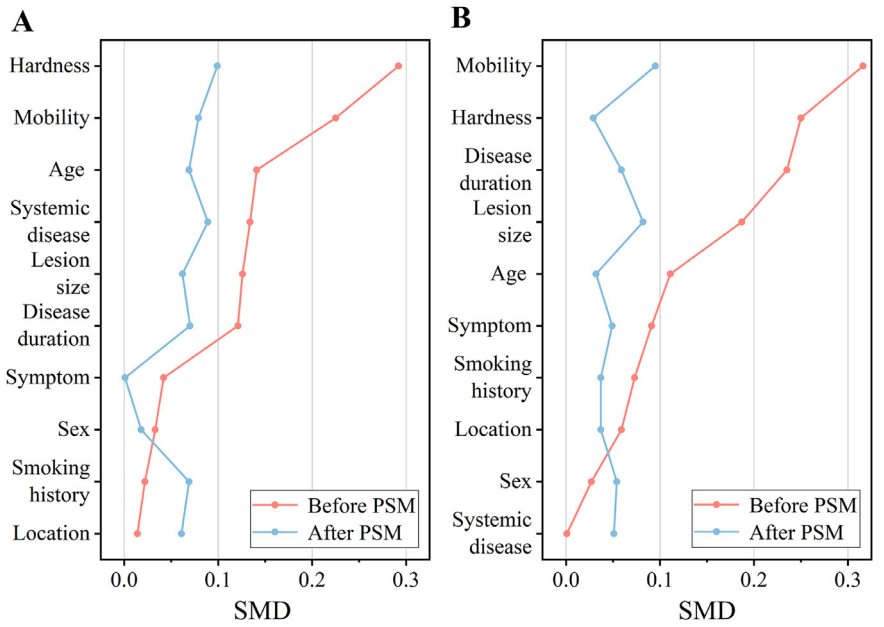

Fig. 1. Covariate balance measured separately by standardized mean difference in **(A)** the pleomorphic adenoma cohort and **(B)** the Warthin tumor cohort before and after propensity score matching, arranged by parameters in decreasing size of standardized mean difference before PSM. PSM, propensity score matching.

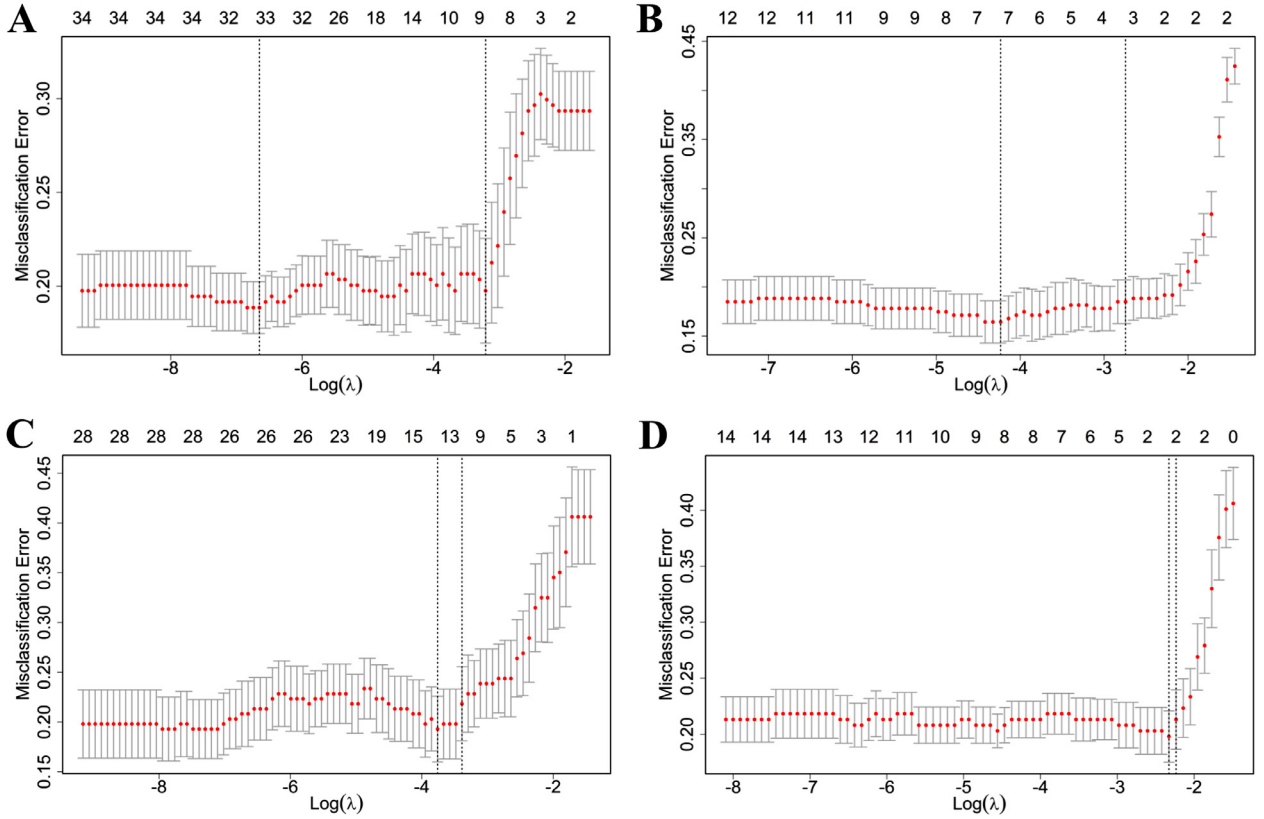

Fig. 2. Radiomic feature selection using a least absolute shrinkage and selection operator (LASSO) regression model. We used 10-fold cross-validation in the LASSO model for the selection of the conditioning parameters (λ). The misclassification error was plotted against log (λ) by using the minimum standard and the minimum standard of standard error (1 − SE standard) to draw the vertical line with the best value. λ values of 0.040, 0.053, 0.059, and 0.129, with log (λ) values of −3.219, −2.737, −3.504, and −2.225, were chosen according to the 10-fold cross-validation separately. **(A)** Group A; **(B)** group B; **(C)** group C; **(D)** group D.

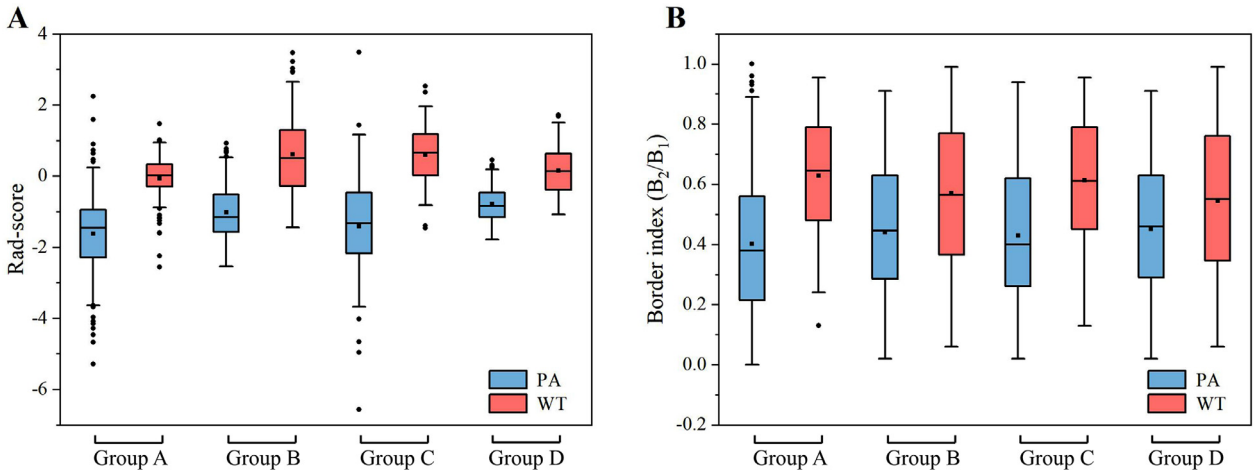

Fig. 3. Box-and-whisker plots of **(A)** radiomic signature (rad-score) and **(B)** border index for patients in groups A, B, C, and D, separately, showing significant differences between patients with pleomorphic adenomas and Warthin tumors ($P < .05$). Horizontal line in the box, median; upper and lower limits of the box, 1.5 × the interquartile range above and below the median; dots, outliers.

Based on the obtained radiomic features, the rad-scores were calculated (Supplementary Materials, available at [URL/link]). The patients' rad-scores are shown as a waterfall plot (Supplementary Figure S1, available at [URL/link]). Data regarding the mean rad-scores for patients in the 4 groups in distinguishing PA and WT are presented in Figure 3A; similarly, data regarding the border index are presented in Figure 3B.

ROC data regarding the rad-score signature of MRI and CT before PSM (groups A and B, respectively) are presented in Figure 4A; the ROC MRI and CT data after PSM (groups C and D, respectively) are presented in Figure 4B. ROC data regarding the border index of MRI and CT before PSM (groups A and B, respectively) are presented in Figure 4C; the ROC MRI and CT data after PSM (groups C and D, respectively) are presented in Figure 4D. The mean rad-score for patients with WT was significantly higher than that for patients with PA in all 4 groups ($P < .05$; Figure 3A). Before PSM, the rad-score signatures had AUCs of 0.895 (95% confidence interval [CI], 0.857-0.932) and 0.897 (95% CI, 0.861-0.932) in group A (MRI) and group B (CT), respectively (Table I). By using the DeLong test, they were found to be similar ($P > .05$; Figure 4A). After PSM, the AUCs of the rad-score to differentiate between PA and WT were 0.911 (95% CI, 0.871-0.951) for MRI (group C) and 0.876 (95% CI, 0.829-0.923) for CT (group D) (Table I); there was no statistical difference between them ($P > .05$; Figure 4B).

The patients' border index values are shown in Supplementary Figure S2 (available at [URL/link]). The mean border index values for patients with WT were significantly higher than those for patients with PA ($P < .05$) in all 4 groups (Figure 3B). Before PSM, the border index in group A (MRI) and group B (CT) had AUCs of 0.760 (95% CI, 0.707-0.813) and 0.652 (95% CI, 0.589-0.716), respectively, with the border index in group A (MRI) being significantly larger than that in group B (CT), as shown in Table I and Figure 4C ($P < .05$). After PSM, the AUCs of the border index to differentiate PA and WT were 0.716 (95% CI, 0.646-0.787) for MRI (group C) and 0.608 (95% CI, 0.527-0.690) for CT (group D), with the AUC for MRI being significantly larger than that for CT ($P < .05$; Table I and Figure 4D). Almost all values that indicated the classification performance (accuracy, sensitivity, specificity, positive predictive value, and negative predictive value) were higher for rad-scores in all 4 cohort groups than for the corresponding border indices. Details of these parameters are shown in Table I. Representative examples of border detection in the 4 study groups are presented in Figure 5.

DISCUSSION

PA has a high risk of malignant transformation and recurrence[4-6]; thus, an aggressive surgical approach is necessary for management.[7] Lateral or complete parotid resection is performed, although it has a high risk of facial nerve injury.[8] In contrast, more conservative resection should be performed for WT because of the low frequency of malignant transformation and low recurrence risk.[9] Therefore, PAs and WTs must be accurately differentiated. Our results indicated that MRI provides more information than CT regarding the margin appearances of PAs and WTs, though no difference was found between the radiomic features of the 2 lesions. These conclusions can be used for consideration or reference when clinicians recommend patients for a preoperative examination.

Among the preoperative imaging examinations for parotid tumors, CT provides good anatomic resolution,

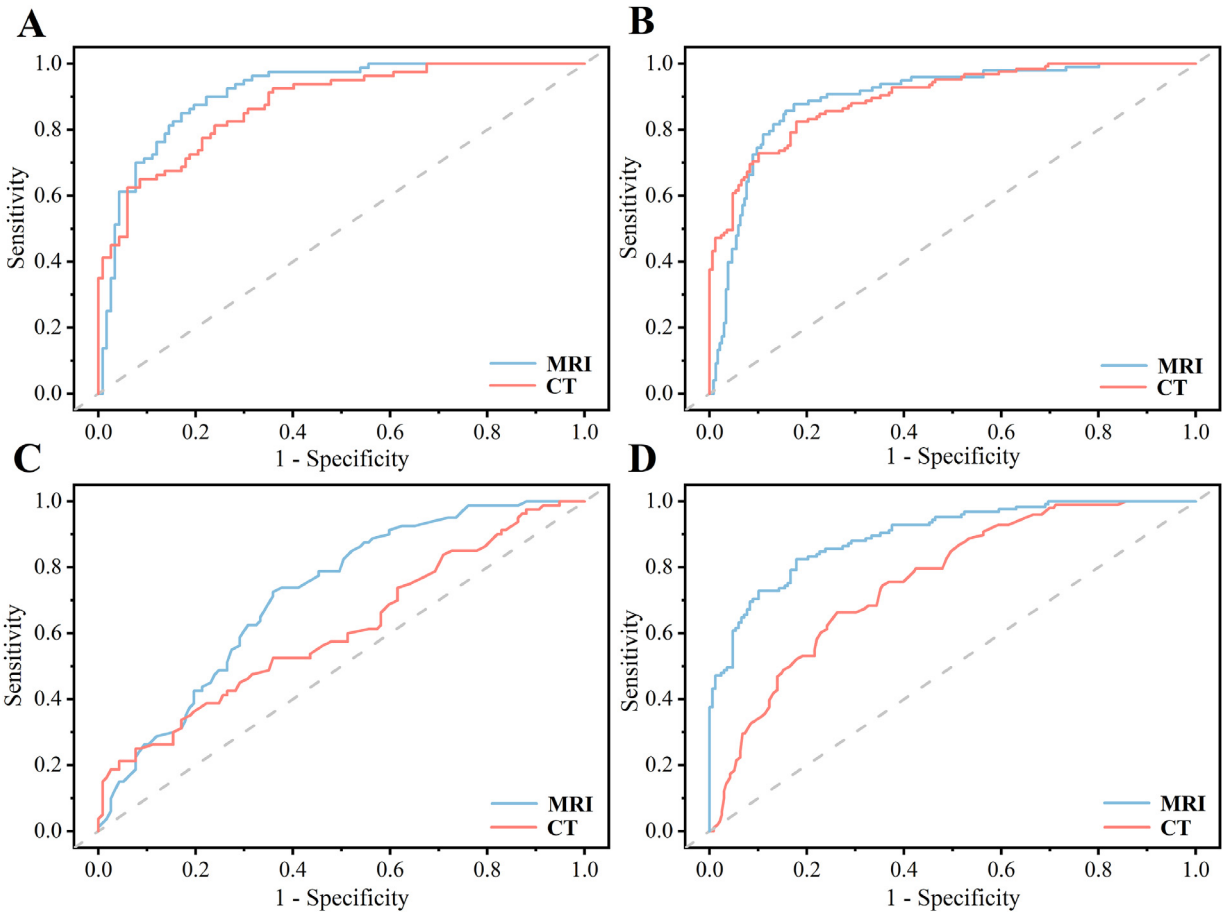

Fig. 4. Receiver operating characteristic curves of the radiomic signatures (rad-scores) and border indices of magnetic resonance imaging (MRI) and computed tomography (CT). **(A)** Rad-score signature before propensity score matching (PSM). The MRI data represent group A and the CT data represent group B. **(B)** Rad-score signature after PSM. The MRI data represent group C and the CT data represent group D. **(C)** Border index before PSM. The MRI data represent group A and the CT data represent group B. **(D)** Border index after PSM. The MRI data represent group C and the CT data represent group D.

soft tissue contrast, and detailed morphology, and thereby revolutionized the radiologic examination of salivary gland masses in the early 1980s. Nevertheless, MRI has tended to replace conventional CT in preoperative assessments because of the absence of radiation, lack of requirement for iodine-containing contrast material, and excellent contrast differentiation. In the present study, by applying radiomics and an image processing algorithm, we attempted to evaluate these 2 imaging approaches from a more objective and quantitative perspective. Specifically, texture analysis was performed to extract high-throughput data by characterizing intratumoral heterogeneity on MR and CT images.

The diagnostic value of well- or ill-defined tumor margins on images appears controversial because this assessment depends on the radiologist's personal experiences.[28]

Table I. Predictive performance of rad-score and border index (B_2/B_1)

	Rad-score						*Border index (B_2/B_1)*					
	AUC (95% CI)	*ACC (%)*	*SENS (%)*	*SPEC (%)*	*PPV (%)*	*NPV (%)*	*AUC (95% CI)*	*ACC (%)*	*SENS (%)*	*SPEC (%)*	*PPV (%)*	*NPV (%)*
Group A	0.895 (0.857-0.932)	84.1	87.8	82.6	67.7	94.2	0.760 (0.707-0.813)	71.6	66.3	73.7	51.2	84.1
Group B	0.897 (0.861-0.932)	82.3	82.4	82.1	77.4	86.3	0.652 (0.589-0.716)	64.4	37.1	84.5	63.9	64.5
Group C	0.911 (0.871-0.951)	83.8	85.0	82.9	77.3	89.0	0.716 (0.646-0.787)	67.5	72.5	64.1	58.0	77.3
Group D	0.876 (0.829-0.923)	78.2	81.3	76.1	69.9	85.6	0.608 (0.527-0.690)	65.0	25.0	92.3	69.0	64.3

AUC, area under the receiver operating characteristic curve; *CI*, confidence interval; *ACC*, accuracy; *SENS*, sensitivity; *SPEC*, specificity; *PPV*, positive predictive value; *NPV*, negative predictive value.

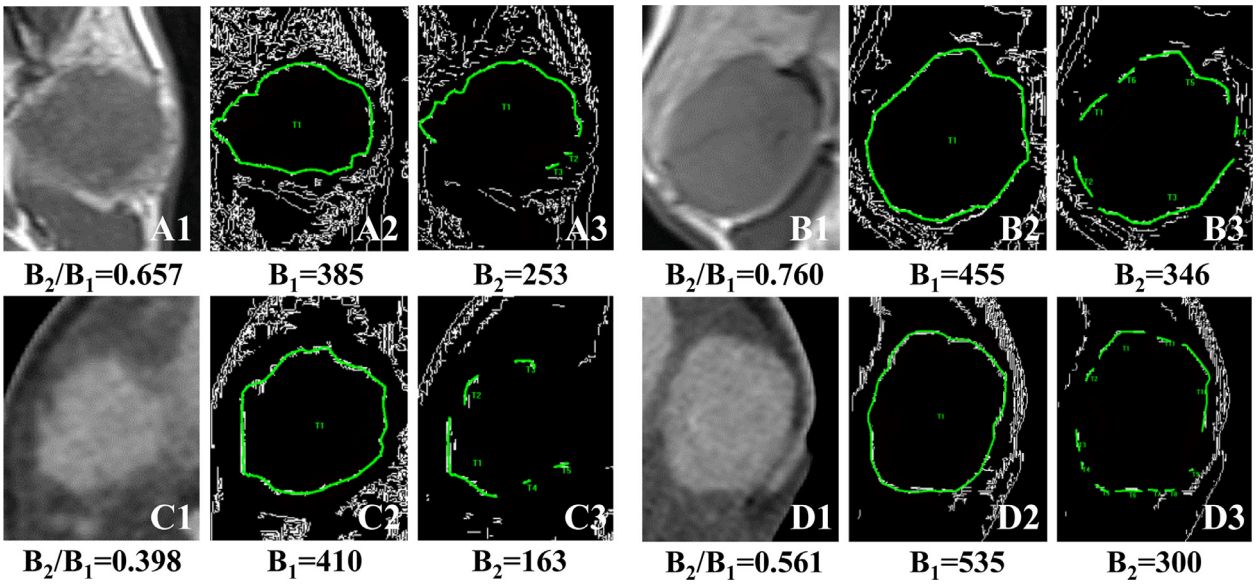

Fig. 5. Representative example of border detection procedure by Canny edge detection. **(A1)** T1-weighted magnetic resonance image of a pleomorphic adenoma; **(B1)** T1-weighted magnetic resonance image of a Warthin tumor; **(C1)** Computed tomographic image of a pleomorphic adenoma; **(D1)** Computed tomographic image of a Warthin tumor. The whole tumor border (B_1) was detected with the parameters of 40/100 [lower threshold (Th1)/higher threshold (Th2)] **(A2), (B2), (C2), (D2)**, and the well-defined border (B_2) was detected at 60/120 (Th1/Th2) **(A3), (B3), (C3), (D3)**.

To facilitate an objective quantitative analysis, we first attempted to quantify the tumor border definition by adjusting the double threshold using Canny edge detection. This algorithm is widely applied for tumor region detection, achieving desirable image segmentation.[29] Using a multistage algorithm to detect a wide range of edges in the images, the algorithm can track the locations of the sharpest changes in intensity values in a variety of directions. Histopathological features have shown that PA, unlike WT, usually presents with an incomplete capsule and capsular infiltration of tumor cells.[30] Therefore, the Canny edge detection algorithm can be a promising method to differentiate between PA and WT based on the margins on MR and CT images. In this study, lesion texture and margin characteristics were selected as evaluation indicators to compare the effectiveness of MRI and CT in differentiating between PA and WT.

Theoretically, in a prospective study of diagnostic efficacy, several radiologic images of each case should be acquired for radiographic intrasubject comparison. However, in real clinical settings, most patients only undergo one examination because of economic or ethical reasons, thus making intergroup comparability an important reference factor in diagnostic radiology research.

Before comparing the diagnostic efficacy between MRI and CT, it is particularly important to first identify the potential confounders. Some clinicians, for instance, may be more inclined to use MRI if a malignant parotid tumor is highly suspected. Such a situation could result in MRI being performed for many patients with relatively harder, larger, and less mobile masses. Other physicians might refer older patients for CT because they are generally less cooperative during the imaging examination (such as having difficulty with respiratory control), and patient cooperation is more important during MRI than during CT examination. In addition, patients with systemic diseases are usually assigned based on the subjective judgment of the treating clinician. Consequently, in a retrospective analysis, uneven distribution of various clinical factors might occur, which may potentially affect the diagnostic efficacy between groups.

In recent years, PSM has played an important role in avoiding confounder bias, thus minimizing the limitations of retrospective studies. It is a powerful tool to simulate the randomization process in randomized controlled trials (RCTs) of a study population. After PSM, it is usually recommended that data be analyzed as if they were paired or repeated measures.[31] However, PSM has not been extensively used to compare different imaging examinations in radiology.[32] In the present study, we used PSM to balance 2 patient groups.

At present, there is very little literature that provides elaboration regarding the quantitative comparison of MRI and CT, especially for parotid tumors. The available research has mainly relied on empirical description. A meta-analysis conducted in 2014 showed that there was no statistically significant difference between MRI and CT in diagnosing salivary gland tumors

clinically.[33] According to the current research, the diagnosis of a parotid tumor by MRI and CT is based on the same histopathological characteristics.

PAs frequently exhibit myxoid or chondroid matrices, in which the extracellular matrix is rich in free water, leading to a higher signal intensity than that for WTs on T2-weighted images. WTs have the highest microvascularity among all parotid tumors, showing a higher degree of enhancement on CT images.[2] Furthermore, focal dystrophic calcifications, which cannot be viewed on MRI, are better appreciated on CT. Calcifications strongly suggest a diagnosis of PA, because such tumoral calcifications are extremely rare in any other parotid tumor.[34] In the present study, with the application of lesion texture analysis, the above empirical characteristics were converted into pixel arrangements in the image, which were quantified into a logistic regression model; our results were consistent with those of previous research. It is also suggested that MRI provides more information about the contours of a lesion than CT.

Some possible speculations are as follows: On MRI, the lesion contours can be better distinguished from the adjacent parotid and extraparotid tissues, especially on T2-weighted images.[2] The improved soft tissue contrast of MRI also permits better evaluation of the interface between the muscle and tumor.[15] This represents a significant advantage over CT, in which the tumors and muscle have the same density and the accuracy of Canny edge detection can be affected.[35] Moreover, if the fat content of the parotid gland is low, the gray value of the tumor and normal gland tissue on CT images would become very similar as the density difference is reduced.[23] Often, in such cases, it is not possible to recognize the tumor boundary, either by using Canny edge detection or merely by a professional's experience. Koyuncu et al.[23] assessed MRI and CT results with respect to tumor margin characteristics and infiltration of surrounding tissue, performed by 2 radiologists independently. The results indicated that the specificity of MRI was higher than that of CT for tumor margin characteristics, which also supports the conclusion of our qualitative analysis.

According to the results of the present investigation, most values reflecting the classification performance in all 4 cohort groups were higher for rad-scores than for the corresponding border indices, indicating that texture analysis on MRI/CT may provide more diagnostic information than analysis of tumor margins. However, more research needs to be carried out to confirm this conclusion with the emergence of new algorithms (e.g., algorithms reflecting the distribution of "sharp" margins). In clinical practice, owing to the malignant transformation and high recurrence risks of PA compared with WT, it is more important not to miss the diagnosis of PA. Therefore, high specificity and positive predictive value are necessary. In the present study, our results showed that the specificity values (82.9%) and positive predictive value (77.3%) of the rad-score in MRI were higher compared with CT (76.1% and 69.9%, respectively), which indicated that for a patient highly suspected of having PA, MRI examination would be preferred.

This was a preliminary research of serial studies. In the future, we may achieve more reliable diagnoses by including the advantages of MRI and CT with computer-assisted quantitative image evaluation. Some limitations of this study are worth noting. First, PSM mimics RCTs, allowing investigators to perform data analysis with reduced concerns of confounding factors. However, RCTs are still the gold standard level of evidence; thus, more research is needed to support our conclusions. Second, this was only a preliminary study comparing the diagnostic performance of MRI and CT. The predictive performance (calibration and discrimination) of the model should be measured. Internal and external validations are also needed to adjust the model for overfitting and quantify any optimism. Finally, to obtain a comprehensive evaluation, future work should take into consideration more indices, such as tumor shape and growth pattern, on MRI and CT images.

CONCLUSION

Tumor radiomic features and margin appearance on MRI and CT images have diagnostic value in differentiating PA from WT. We found no difference between MRI and CT for comparison based on radiomic features; however, our results showed that MRI was more informative with respect to the tumor margin appearance. An analysis of the original data before PSM produced similar results. MRI appears to be a better preoperative examination technique for diagnosing PA and WT. However, more research is needed to validate our conclusions.

DISCLOSURE

All procedures involving human participants in the present study were performed in accordance with the ethical standards of the institutional research committee and with the 1964 Declaration of Helsinki and its later amendments or comparable ethical standards.

SUPPLEMENTARY MATERIALS

Supplementary material associated with this article can be found in the online version at doi:10.1016/j.oooo.2021.01.014.

REFERENCES

1. Shao S, Mao N, Liu W, et al. Epithelial salivary gland tumors: utility of radiomics analysis based on diffusion-weighted

imaging for differentiation of benign from malignant tumors. *J Xray Sci Technol*. 2020;28:799-808.
2. Okahara M, Kiyosue H, Hori Y, Matsumoto A, Mori H, Yokoyama S. Parotid tumors: MR imaging with pathological correlation. *Eur Radiol*. 2003;13:25-33.
3. Cardesa A, Slootweg PJ, Gale N, Franchi A. *Benign and potentially malignant lesions of the squamous epithelium and squamous cell carcinoma*. Pathology of the Head and Neck. Berlin, Germany: Springer; 2016:1-48.
4. Maran AG, Mackenzie IJ, Stanley RE. Recurrent pleomorphic adenomas of the parotid gland. *Arch Otolaryngol*. 1984;110: 167-171.
5. Som PM, Curtin HD. *Salivary glands. Anatomy and pathology*. Head and Neck Imaging. Missouri: Mosby; 2003:2097-2098.
6. Antony J, Gopalan V, Smith RA, Lam AKY. Carcinoma ex pleomorphic adenoma: a comprehensive review of clinical, pathological and molecular data. *Head Neck Pathol*. 2012;6:1-9.
7. Park SJ, Han S, Lee HJ, Ahn SH, Jeong WJ. Preservation of salivary function following extracapsular dissection for tumors of the parotid gland. *J Oral Maxillofac Surg*. 2018;76:2004-2010.
8. O'Brien CJ. Current management of benign parotid tumors—the role of limited superficial parotidectomy. *Head Neck*. 2003;25: 946-952.
9. Heller KS, Attie JN. Treatment of Warthin's tumor by enucleation. *Am J Surg*. 1988;156:294-296.
10. Yologlu Z, Aydin H, Alp NA, Aribas BK, Kizilgoz V, Arda K. Diffusion weighted magnetic resonance imaging in the diagnosis of parotid masses. *Saudi Med J*. 2016;37:1412.
11. Karaman Y, Özgür A, Apaydın D, Özcan C, Arpacı R, Duce MN. Role of diffusion-weighted magnetic resonance imaging in the differentiation of parotid gland tumors. *Oral Radiol*. 2016;32:22-32.
12. Urquhart A, Hutchins LG, Berg RL. Preoperative computed tomography scans for parotid tumor evaluation. *Laryngoscope*. 2001;111:1984-1988.
13. Kim KH, Sung MW, Yun JB, et al. The significance of CT scan or MRI in the evaluation of salivary gland tumors. *Auris Nasus Larynx*. 1998;25:397-402.
14. Kato H, Kanematsu M, Watanabe H, Mizuta K, Aoki M. Salivary gland tumors of the parotid gland: CT and MR imaging findings with emphasis on intratumoral cystic components. *Neuroradiology*. 2014;56:789-795.
15. Lee YYP, Wong KT, King AD, Ahuja AT. Imaging of salivary gland tumours. *Eur J Radiol*. 2008;66:419-436.
16. Yu H. Automated Segmentation of Head and Neck Cancer Using Texture Analysis with Co-registered PET/CT images. 2010. http://hdl.handle.net/1807/24920. Accessed 2 Sep 2010.
17. Matzner-Lober E, Suehs CM, Dohan A, Molinari N. Thoughts on entering correlated imaging variables into a multivariable model: application to radiomics and texture analysis. *Diagn Interv Imaging*. 2018;99:269-270.
18. Zhang D, Li X, Lv L, et al. Improving the diagnosis of common parotid tumors via the combination of CT image biomarkers and clinical parameters. *BMC Med Imaging*. 2020;20:1-9.
19. Sollini M, Antunovic L, Chiti A, Kirienko M. Towards clinical application of image mining: a systematic review on artificial intelligence and radiomics. *Eur J Nucl Med Mol Imaging*. 2019;10:1-17.
20. Zhang Z, Song C, Zhang Y, Wen B, Zhu J, Cheng J. Apparent diffusion coefficient (ADC) histogram analysis: differentiation of benign from malignant parotid gland tumors using readout-segmented diffusion-weighted imaging. *Dentomaxillofac Radiol*. 2019;48:20190100.
21. Areiza-Laverde HJ, Malpica-González N, Brea B, Castro-Ospina AE, Díaz GM. Radiomics-based differentiation of pleomorphic adenomas and Warthin tumors of salivary glands. In: *Paper presented at: 15th International Symposium on Medical Information Processing and Analysis, Medelin, Colombia*; 2020.
22. Schaefer SD, Close LG, Maravilla KR, Suss RA, Merkel MA, Burns DK. Evaluation of NMR versus CT for parotid masses: a preliminary report. *Laryngoscope*. 1985;95:945-950.
23. Koyuncu M, Şeşen T, Akan H, et al. Comparison of computed tomography and magnetic resonance imaging in the diagnosis of parotid tumors. *Otolaryngol Head Neck Surg*. 2003;129:726-732.
24. Preetha J, Selvarajan S, Suresh P. Comparative analysis of various image edge detection techniques for two dimensional CT scan neck disc image. *Int J Comput Sci Commun*. 2012;3:57-61.
25. Green B. Canny Edge Detection Tutorial. http://dasl.mem.drexel.edu/alumni/bGreen/www.pages.drexel.edu/-weg22/cantut.html. Accessed 20 Oct 2010.
26. Fruehwald-Pallamar J, Czerny C, Holzer-Fruehwald L, et al. Texture-based and diffusion-weighted discrimination of parotid gland lesions on MR images at 3.0 Tesla. *NMR Biomed*. 2013;26:1372-1379.
27. Huang Y, Liu Z, He L, et al. Radiomics signature: a potential biomarker for the prediction of disease-free survival in early-stage (I or II) non-small cell lung cancer. *Radiology*. 2016;281:947-957.
28. Vogl TJ, Albrecht MH, Nour-Eldin N-E-dA, et al. Assessment of salivary gland tumors using MRI and CT: impact of experience on diagnostic accuracy. *Radiol Med*. 2018;123:105-116.
29. Hazra A, Dey A, Gupta SK, Ansari MA. Brain tumor detection based on segmentation using MATLAB. In: *Paper presented at: 1-2 Aug. 2017 International Conference on Energy, Communication, Data Analytics and Soft Computing (ICECDS), Chennai*; 2017.
30. Lopes MLDdS, Barroso KMA, Henriques ÁCG, dos Santos JN, Martins MD, de Souza LB. Pleomorphic adenomas of the salivary glands: retrospective multicentric study of 130 cases with emphasis on histopathological features. *Eur Arch Otorhinolaryngol*. 2017;274:543-551.
31. Baek S, Park SH, Won E, Park YR, Kim HJ. Propensity score matching: a conceptual review for radiology researchers. *Korean J Radiol*. 2015;16:286-296.
32. McDonald RJ, McDonald JS, Kallmes DF, Carter RE. Behind the numbers: propensity score analysis—a primer for the diagnostic radiologist. *Radiology*. 2013;269:640-645.
33. Liu Y, Li J, Tan Y-r, Xiong P, Zhong LP. Accuracy of diagnosis of salivary gland tumors with the use of ultrasonography, computed tomography, and magnetic resonance imaging: a meta-analysis. *Oral Surg Oral Med Oral Pathol Oral Radiol*. 2015;119:238-245.
34. Som PM, Shugar J, Sacher M, Stollman AL, Biller HF. Benign and malignant parotid pleomorphic adenomas: CT and MR studies. *J Comput Assist Tomogr*. 1988;12:65-69.
35. Dillon W. Applications of magnetic resonance imaging to the head and neck. *Semin Ultrasound CT MR*. 1986;7:202-215.

Reprint requests:

Tao Zhang
Department of Stomatology
Peking Union Medical College Hospital
Chinese Academy of Medical Sciences and
Peking Union Medical College
No.1 Shuaifuyuan
Wangfujing
Dongcheng District
Beijing 100730
China.
drtzhang@126.com